Acta Crystallographica Section B
Structural Science
ISSN 0108-7681

Study of NH_4^+ in the zeolite phillipsite by combined synchrotron powder diffraction and IR spectroscopy

A. F. Gualtieri

Dipartimento di Scienze della Terra, Università di Modena e Reggio Emilia, Via S. Eufemia 19, 41100 Modena, Italy

Correspondence e-mail: alex@unimo.it

Received 2 August 1999
Accepted 4 February 2000

The Rietveld refinement on synchrotron data of three natural hydrated NH_4^+-exchanged phillipsites with different Si/Al ratios allowed acceptable assignment of the NH_4^+ sites. These phillipsites display the typical monoclinic $P2_1/m$ cell, whose volume increases with increasing numbers of NH_4^+ ions, which are refined in the two sites labelled I and II. Some residual Na^+ is retained in the site labelled II′. Distortion of the Si/Al tetrahedra, which affects some absorption bands in the IR spectra, seems to be mainly due to the distribution of Al in the framework, while the interaction of NH_4^+ with the O atoms of the framework seems to play a minor role. NH_4^+ in both sites acts as a donor in hydrogen bonding with O atoms of the framework and water molecules. NH_4^+ in site I has three H atoms interacting with O atoms of the framework and a number of interactions with water O atoms. In all three samples, monocentric and dicentric connections are formed. NH_4^+ in site II has one H atom interacting with O atoms of the framework and a number of interactions with water O atoms. Two monocentric connections and a quadricentric one were found in sample (1), three dicentric connections and a monocentric one in sample (2), and three monocentric connections and a dicentric one in sample (3).

1. Introduction

Phillipsite [PHI] is a monoclinic zeolite (Gottardi & Galli, 1985) with a framework built up from layers of tetrahedra with eight and four rings located roughly perpendicular to the *a* axis. The layers are vertically linked by four rings forming double crankshafts with the four rings of the layer. Its crystal structure was firstly solved in the space group *B*2*mb* (Sadanaga *et al.*, 1961; Steinfink, 1962), which corresponds to the topological symmetry, and then refined in the space group $P2_1/m$ (Rinaldi *et al.*, 1974) with $a \simeq 9.8$, $b \simeq 14.0$, $c \simeq 8.6$ Å, $\beta \simeq 124^\circ$ and two extraframework sites (I and II). Site I on the mirror plane (010) along one of the larger channels of the type I octagonal prism is usually populated by large-size cations such as K^+ or Ba^{2+}. Site II is in a general position in the cage formed by type II octagonal prisms and adjacent type I octagonal prisms. This site is usually populated by Ca^{2+} and Na^+. The positions of the two sites are shown in Fig. 1.

The present work is part of a research project on the crystal structure of cation-exchanged phillipsites and related physicochemical properties. Three phillipsite samples were selected for the research with Si/(Si + Al) = 0.63, 0.72 and 0.76, respectively. Earlier results (Passaglia *et al.*, 1999; Gualtieri *et al.*, 1999*a*,*b*; Gualtieri, Caputo & Colella, 1999) show that:

(i) site I hosts Cs^+, Ba^{2+}, Sr^{2+} and K^+, and can be fully or partially occupied;

Table 1
Chemical composition from electron microprobe analyses (EPA), refined cells and refinement statistics of NH_4-exchanged phillipsites.

Sample	(1)	(2)	(3)
Formula based on 32 O atoms from EPA	$Na_{0.6}(NH_4)_{5.04}(Al_{5.9}Si_{10.0}O_{32})\cdot 9.1H_2O$	$Na_{0.2}(NH_4)_{4.4}(Al_{4.41}Si_{11.6}O_{32})\cdot 8.1H_2O$	$Na_{0.4}(NH_4)_{3.4}(Al_{3.8}Si_{12.16}O_{32})\cdot 7.8H_2O$
Formula based on 8 O atoms from XRD (Z = 4)	$H_{4.76}N_{1.19}Na_{0.13}Al_{1.50}Si_{2.50}O_8\cdot 1.92H_2O$	$H_{4.04}N_{1.01}Na_{0.10}Al_{1.21}Si_{2.99}O_8\cdot 2.37H_2O$	$H_{3.40}N_{0.85}Na_{0.10}Al_{0.96}Si_{3.04}O_8\cdot 2.59H_2O$
a (Å)	10.0507 (5)	10.0122 (8)	9.95960 (26)
b (Å)	14.2016 (8)	14.1943 (12)	14.2015 (4)
c (Å)	8.7281 (8)	8.7284 (17)	8.7051 (5)
β (°)	125.123 (5)	125.024 (11)	124.9901 (34)
Cell volume (Å^3)	1019.0 (9)	1015.81 (2)	1008.7 (3)
No. of observed reflections	4500	4500	4500
No. of independent reflections	701	701	701
No. of refined parameters	104	104	104
R_p	0.040	0.030	0.037
R_{wp}	0.064	0.047	0.063
$R(F^2)$	0.128	0.090	0.122
χ^2	2.5	1.3	2.3
d	1.67	1.63	1.68

(ii) site II hosts Cs^+, Ba^{2+}, Sr^{2+}, K^+, Ca^{2+} and Na^+, but its occupancy is constantly < 50% to prevent an oversaturation of positive charges over the coordinated framework O atoms. The extra amount of cations may be hosted in site II′, close to site II;

(iii) sites I and II are constantly occupied as they are the templating agents for the crystal growth of phillipsite;

(iv) Na^+ and Ca^{2+}, owing to their small size, cannot populate site I, whereas large cations such as K^+ or Ba^{2+} cannot migrate to site II′, which is mainly occupied by Na^+.

This work deals with the results of a combined synchrotron X-ray diffraction and IR study of the structure of NH_4^+-exchanged phillipsites.

2. Experimental

2.1. Materials

The investigated NH_4^+-exchanged phillipsite samples with their Si/(Si + Al) ratio (R) are:

(i) Vallerano (Rome, Italy) with R = 0.63;

(ii) Perrier (Puy du Dôme, France) with R = 0.72;

(iii) Monte Lungo (M. Berici, Vicenza, Italy) with R = 0.76.

The exchanged forms were obtained following the procedure described by Gualtieri *et al.* (1999*a*). Approximately 500 mg of each sample (grain size < 0.2 mm) was first treated with 200 ml of a 1 N Na^+ solution. The Na^+-exchanged products were in turn treated with a NH_4^+ solution (*ca* 50 mg of zeolite in 100 ml), prepared using Merck 'suprapure' chloride and deionized water. The exchanges were carried out in Teflon tubes, slowly oscillating in an oven at 363 K for 3 weeks with one renewal of the solution after the first week.

The chemical composition of the samples including Na^+ was obtained by the average of several microprobe point analyses performed on the rim and core of 4–5 crystals. Electron probe microanalysis (EPMA) was performed using an ARL-SEMQ instrument operating in the wavelength dispersive mode with 15 kV and 20 nA beam current and a defocused beam of 30 µm in diameter. Natural and synthetic silicates were used as standards and on-line data processing was possible using the

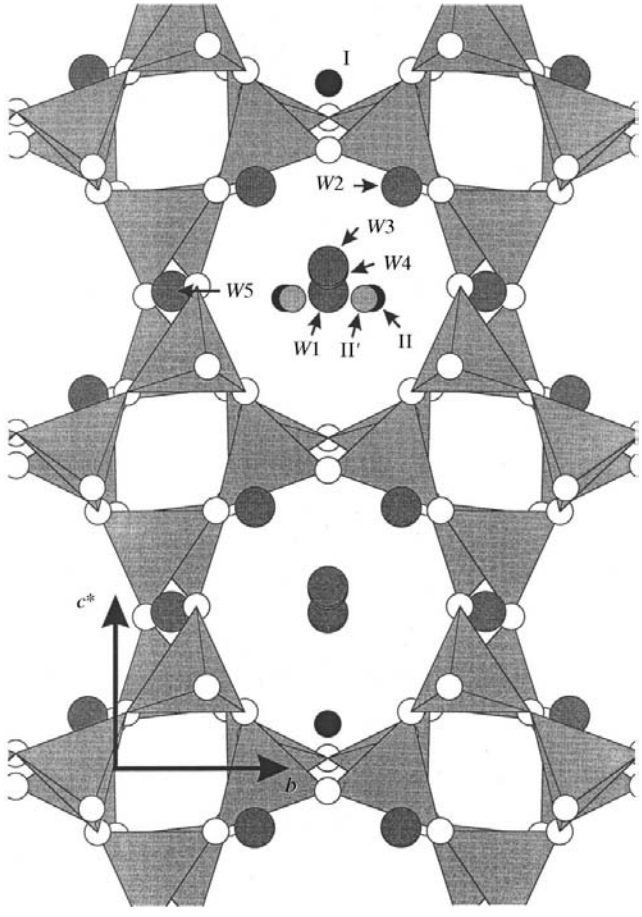

Figure 1
The positions of the extra framework cations in sites I, II and II′, and water molecules in phillipsite.

PROBE program (Donovan, 1995). Microprobe data were normalized to 100 wt% using the contents of NH_4^+ and H_2O determined as the weight loss of the thermogravimetric (TG) analyses. TG analyses were carried out using a SEIKO ssc/5200. Data were collected in air with a heating rate of 10 K min^{-1} in the range 298–1273 K.

2.2. X-ray data collection

Synchrotron powder diffraction data were collected at the X7B beam at the National Synchrotron Light Source (Brookhaven National Laboratory, USA), using a Huber four-circle diffractometer. The X7B beamline geometry is described in detail by Hastings *et al.* (1983). The powders were mounted in a rotating 0.3 mm diameter capillary, on a standard goniometric head and data collected with λ = 1.0047 Å using an Image Plate (IP) detector (Amemija, 1990) mounted on a translating system called a Translating Image Plate System (TIPS; Norby, 1997). The horizontal and vertical beam sizes are 1 and 0.3 mm, respectively. The wavelength was determined using the standard material LaB_6 in a specially developed routine which also allows the calibration of the zero-shift position of the plate, the sample-detector distance and the tilting angle of the IP detector. The exposure time was 10 min and data were collected at low temperature (100 K) using an Oxford cryogenic system in the angular region 2θ = 0–50°. The images stored in the IP were recovered using a Fuji BAS2000 scanner through He–Ne laser stimulation and the extracted powder patterns with a step scan of 2θ = 0.01° were reduced using an original code (Gualtieri *et al.*, 1996; Norby, 1997). The refined region was 2θ = 5–50° (sin θ/λ = 0.51 $Å^{-1}$).

2.3. Refinement and structure analysis

The powder patterns were refined using the *GSAS* software (Larson & Von Dreele, 1999). Starting atomic coordinates for the structural models were taken from Gualtieri *et al.* (1999*b*) and refined in the space group $P2_1/m$. The background profile was fitted with a Chebyshev polynomial function with 18 coefficients in order to correctly fit the bump in the pattern due to the scattering of the glass capillary. The diffraction peak profiles were modelled using a pseudo-Voigt function with one Gaussian and two Lorentzian coefficients. Refinement of the atomic coordinates, the atomic site occupancies for extra framework positions and the isotropic thermal parameters was performed with the aid of soft constraints on tetrahedral bond lengths, which were imposed and used as additional observations in the earlier stages of the refinement and progressively reduced to zero.

Although the distinction of NH_4^+ and H_2O by X-ray diffraction is very hard owing to the similar scattering factors, large thermal parameters and large distances from the framework O atoms (*ca* 2.8 Å), a sound discrimination was possible by comparison with structure refinements of the same samples exchanged with other extraframework cations from Gualtieri *et al.* (1999*a*,*b*). This strategy was successfully adopted by Yang & Armbruster (1998) for the refinement of NH_4^+-exchanged heulandite. The sum of the refined number of atoms per unit cell reasonably matched the total number of NH_4^+ from the TG analysis. Thus, the scattering curve of N^{3+} was utilized for both the refinement of sites I and II in the three structures, while the scattering curve of Na^+ was used for site II′. Rigid-body units were used to model the NH_4^+ ions. The use of rigid bodies has a number of advantages: it permits the inclusion of H atoms in the refinement whose contribution to the profile is clearly measurable (Lightfoot *et al.*, 1993) and drastically reduces the number of refined parameters, which allows refinement with much higher accuracy (Schreinger, 1963). The shift and rotational degree of freedom of the NH_4^+ group, and the N—H and H—H distances were constrained using weights and an overall thermal parameter was refined for each rigid-body unit according to the strategy suggested by Dinnebier (1999).

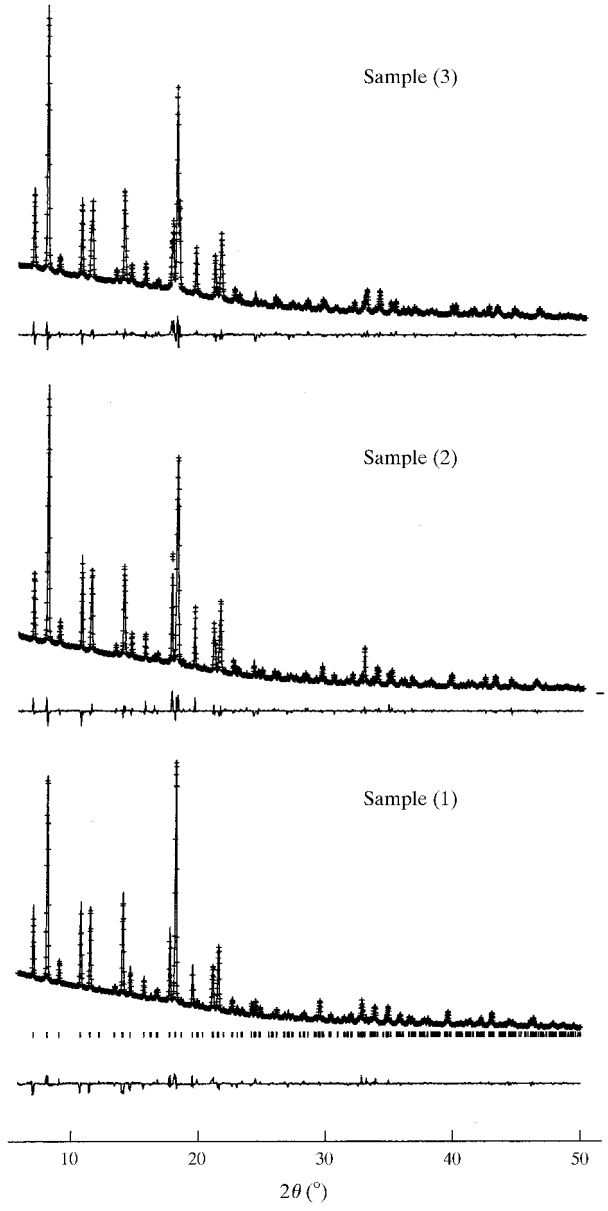

Figure 2
Observed (crosses), calculated (continuous line) and difference curves (bottom line) of the refined patterns.

Table 2
Coordinates, populations and thermal parameters of the framework atoms.

Parentheses in the first column report the site multiplicity, while parentheses in the other columns are the standard deviation.

Site	Sample (1)	Sample (2)	Sample (3)
*T*1			
x	0.7449 (2)	0.7363 (3)	0.7285 (5)
y	0.0244 (4)	0.0193 (4)	0.0155 (4)
z	0.2906 (2)	0.2960 (3)	0.2797 (2)
Occ.	1.0	1.0	1.0
U_{iso}	0.042 (8)	0.037 (9)	0.042 (7)
*T*2			
x	0.4213 (3)	0.4250 (2)	0.4171 (3)
y	0.1383 (5)	0.1390 (5)	0.1364 (6)
z	0.0063 (4)	0.0160 (3)	0.0149 (5)
Occ.	1.0	1.0	1.0
U_{iso}	0.035 (8)	0.045 (7)	0.041 (7)
*T*3			
x	0.0555 (3)	0.0462 (4)	0.0591 (3)
y	0.0055 (4)	0.0106 (4)	0.0110 (3)
z	0.2814 (3)	0.2745 (3)	0.2951 (3)
Occ.	1.0	1.0	1.0
U_{iso}	0.027 (7)	0.041 (8)	0.042 (8)
*T*4			
x	0.1249 (3)	0.1204 (6)	0.1129 (2)
y	0.1335 (6)	0.1345 (3)	0.1403 (5)
z	0.0479 (4)	0.0359 (4)	0.0294 (4)
Occ.	1.0	1.0	1.0
U_{iso}	0.031 (9)	0.032 (9)	0.047 (9)
O1			
x	0.1390 (4)	0.0805 (4)	0.0686 (2)
y	0.0872 (3)	0.1034 (4)	0.0914 (1)
z	0.2256 (3)	0.1874 (3)	0.1671 (2)
Occ.	1.0	1.0	1.0
U_{iso}	0.039 (8)	0.051 (7)	0.064 (7)
O2			
x	0.6503 (5)	0.6461 (3)	0.6626 (3)
y	0.5724 (4)	0.5782 (3)	0.5928 (3)
z	0.1807 (2)	0.1759 (2)	0.1944 (2)
Occ.	1.0	1.0	1.0
U_{iso}	0.020 (8)	0.021 (9)	0.020 (8)
O3			
x	0.6106 (3)	0.5992 (4)	0.6020 (3)
y	0.1059 (4)	0.1032 (5)	0.1067 (4)
z	0.1684 (3)	0.2033 (5)	0.1989 (4)
Occ.	1.0	1.0	1.0
U_{iso}	0.051 (9)	0.066 (9)	0.049 (8)
O4			
x	0.0155 (3)	0.0136 (3)	0.0174 (5)
y	0.9110 (1)	0.9095 (5)	0.9241 (5)
z	0.1607 (2)	0.1728 (3)	0.1521 (3)
Occ.	1.0	1.0	1.0
U_{iso}	0.077 (9)	0.047 (8)	0.044 (8)
O5			
x	0.8952 (4)	0.8849 (4)	0.8879 (3)
y	0.0517 (3)	0.0444 (4)	0.0401 (4)
z	0.2667 (3)	0.2703 (4)	0.2763 (5)
Occ.	1.0	1.0	1.0
U_{iso}	0.037 (9)	0.064 (7)	0.083 (7)
O6			
x	0.3222 (3)	0.3113 (4)	0.3099 (3)
y	0.3749 (6)	0.3774 (6)	0.3736 (4)
z	0.1146 (5)	0.1023 (3)	0.1054 (4)
Occ.	1.0	1.0	1.0
U_{iso}	0.039 (8)	0.037 (8)	0.037 (9)
O7			
x	0.7964 (3)	0.7988 (3)	0.7839 (3)
y	0.4688 (4)	0.4866 (5)	0.4858 (2)
z	0.5090 (3)	0.5153 (2)	0.4949 (1)
Occ.	1.0	1.0	1.0
U_{iso}	0.037 (8)	0.036 (9)	0.021 (9)
O8			
x	0.5710 (2)	0.5661 (1)	0.5640 (2)
y	0.7500	0.7500	0.7500
z	0.0610 (2)	0.0415 (3)	0.0190 (2)
Occ.	1.0	1.0	1.0
U_{iso}	0.090 (8)	0.091 (7)	0.077 (8)
O9			
x	0.0755 (3)	0.0834 (2)	0.0390 (3)
y	0.2500	0.2500	0.2500
z	0.0269 (2)	0.0242 (2)	0.0110 (3)
Occ.	1.0	1.0	1.0
U_{iso}	0.051 (8)	0.033 (9)	0.023 (9)

The agreement indices for the final least-squares cycles of all refinements are reported in Table 1 together with the composition of the samples and cell constants. Fig. 2 shows the observed (crosses), calculated (continuous line) and difference curves (bottom line) of the refined patterns.[1]

2.4. IR spectroscopy

Pellets of the powder sample were obtained using the KBr wafer technique and data were collected at room temperature between 400 and 4000 cm^{-1} using a Bruker spectrometer, model IFS 113 V, with a resolution of 1 cm^{-1}. Raw spectra were reduced using the Bruker acquisition software, which enabled the baseline correction and normalization of the data.

3. Results

Cation exchange with NH_4^+ can be considered complete in phillipsite, although some sodium determined from the microprobe analysis is retained. Table 1 reports the chemical composition of the phillipsite samples as determined by EPMA. The chemical composition of course reports the NH_4^+ and H_2O contents determined by the TG analyses. Since the discrimination of NH_4^+ and H_2O in the TG analysis is based on the sound but arbitrary proviso that the weight loss attributed to NH_4^+ is at $T > 673$ K, we expect some difference between the water and NH_4^+ contents calculated from the refinements.

Table 2 reports the refined coordinates of the framework while Table 3 reports those of the extraframework cations, their populations and thermal parameters of the three structures refined in the space group $P2_1/m$. The occupancy of site I and that of some water molecules was fixed to unity, since the refined values were very close to 1. The number of refined

[1] Supplementary data for this paper are available from the IUCr electronic archives (Reference: NA0099). Services for accessing these data are described at the back of the journal.

Table 3
Coordinates, populations and thermal parameters of the extra framework cations.

Parentheses in the first column report the site multiplicity, while parentheses in the other columns are the standard deviation.

Site	Sample (1)	Sample (2)	Sample (3)
N in I(2)†			
x	0.8753 (3)	0.8791 (4)	0.871 (1)
y	1/4	1/4	1/4
z	0.1716 (3)	0.1898 (4)	0.194 (1)
Occ.	1.0‡	1.0‡	1.0‡
U_{iso}	0.08 (1)	0.07 (1)	0.07 (1)
N in II(4)†			
x	0.4068 (3)	0.4599 (4)	0.460 (1)
y	0.6891 (2)	0.7052 (5)	0.7052 (6)
z	0.488 (4)	0.5066 (7)	0.5064 (5)
Occ.	0.69 (3)	0.51 (4)	0.35 (4)
U_{iso}	0.037 (7)	0.06 (1)	0.05 (1)
Na in II′(4)			
x	0.6763 (3)	0.6733 (5)	0.659 (4)
y	0.1923 (2)	0.1652 (7)	0.164 (1)
z	0.455 (4)	0.5162 (5)	0.506 (4)
Occ.	0.13 (4)	0.10 (3)	0.10 (4)
U_{iso}	0.03 (1)	0.09 (1)	0.06 (1)
O(*W*1) (2)			
x	0.7637 (3)	0.7005 (4)	0.7117 (2)
y	3/4	3/4	3/4
z	0.4462 (4)	0.4136 (5)	0.4377 (4)
Occ.	1.0‡	0.95 (3)	1.0‡
U_{iso}	0.04 (1)	0.02 (1)	0.04 (2)
O(*W*2) (2)			
x	0.9499 (2)	0.8994 (4)	0.8775 (3)
y	1/4	1/4	1/4
z	0.5546 (3)	0.5411 (3)	0.5133 (5)
Occ.	1.0‡	1.0‡	1.0‡
U_{iso}	0.08 (1)	0.06 (1)	0.08 (1)
O(*W*3) (4)			
x	0.376 (1)	0.3121 (2)	0.352 (6)
y	0.805 (1)	0.8691 (7)	0.8636 (8)
z	0.154 (2)	0.1233 (4)	0.106 (2)
Occ.	0.5§	0.62 (5)	0.73 (4)
U_{iso}	0.06 (1)	0.08 (1)	0.09 (1)
O(*W*4) (2)			
x	0.464 (1)	0.7058 (7)	0.686 (4)
y	1/4	1/4	1/4
z	0.501 (2)	0.7920 (5)	0.777 (2)
Occ.	0.11 (2)	0.55 (3)	0.72 (3)
U_{iso}	0.08 (1)	0.08 (1)	0.08 (1)
O(*W*5) (4)			
x	1/2	1/2	1/2
y	1/2	1/2	1/2
z	1/2	1/2	1/2
Occ.	0.73 (4)	1.0‡	1.0‡
U_{iso}	0.09 (2)	0.07 (1)	0.08 (1)
HI1(2)†			
x	0.853 (3)	0.881 (3)	0.903 (1)
y	1/4	1/4	1/4
z	0.258 (2)	0.2947 (9)	0.313 (1)
Occ.	1.0‡	1.0‡	1.0‡
U_{iso}	0.05 (2)¶	0.06 (2)¶	0.06 (3)¶
HI2(2)†			
x	0.984 (8)	0.982 (8)	0.961 (1)
y	1/4	1/4	1/4
z	0.230 (3)	0.221 (5)	0.194 (1)
Occ.	1.0‡	1.0‡	1.0‡
U_{iso}	0.05 (2)¶	0.06 (2)¶	0.06 (3)¶
HI3(4)†			
x	0.832 (1)	0.826 (1)	0.811 (9)
y	0.302 (1)	0.302 (1)	0.302 (1)
z	0.099 (4)	0.122 (3)	0.136 (1)
Occ.	1.0‡	1.0‡	1.0‡
U_{iso}	0.05 (2)¶	0.06 (2)¶	0.06 (3)¶
HII1(4)†			
x	0.321 (1)	0.371 (1)	0.375 (1)
y	0.723 (1)	0.727 (1)	0.730 (1)
z	0.463 (2)	0.501 (5)	0.5011 (9)
Occ.	0.69 (3)	0.51 (4)	0.35 (4)
U_{iso}	0.05 (2)¶	0.06 (2¶	0.06 (3)¶
HII2(4)†			
x	0.425 (2)	0.531 (1)	0.531 (1)
y	0.642 (8)	0.679 (3)	0.679 (1)
z	0.567 (2)	0.620 (1)	0.621 (1)
Occ.	0.69 (3)	0.51 (4)	0.35 (4)
U_{iso}	0.05 (2)¶	0.06 (2)§	0.06 (3)¶
HII3(4)†			
x	0.495 (1)	0.511 (1)	0.511 (1)
y	0.727 (1)	0.7523 (1)	0.723 (1)
z	0.542 (2)	0.488 (2)	0.485 (1)
Occ.	0.69 (3)	0.51 (4)	0.35 (4)
U_{iso}	0.05 (2)¶	0.06 (2)¶	0.06 (3)¶
HII4(4)†			
x	0.386 (2)	0.426 (1)	0.423 (1)
y	0.665 (1)	0.659 (1)	0.660 (1)
z	0.381 (2)	0.416 (1)	0.418 (1)
Occ.	0.69 (3)	0.51 (4)	0.35 (4)
U_{iso}	0.05 (2)¶	0.06 (2)¶	0.06 (3)¶

† Rigid-body refinement (see text for details). ‡ Fixed to 1.0 since the refined value was very close to unity. § Fixed to 0.5 since the refined value was very close to this value. ¶ Overall thermal parameters for that atomic species.

NH_4^+ is in very good agreement with the amount of NH_4^+ from the TG analysis: refined NH_4^+ is 4.76 atoms per formula unit (a.f.u.) *versus* 5.04 a.f.u. in sample (1); 4.04 a.f.u. *versus* 4.4 a.f.u. in sample (2); 3.40 a.f.u. *versus* 3.40 a.f.u. in sample (3), respectively. Table 4 shows the tetrahedral bond distances and interactions of the NH_4^+ with the framework O atoms and water molecules. The number of refined water molecules is overestimated with respect to the value from the TG analysis. It has already been remarked that the weight loss from TG below 673 K has been attributed to water, while the weight loss above 673 K has been attributed to NH_4^+. It is thus possible that some water lost above 673 K was erroneously attributed to NH_4^+. Refined water molecules are 9.28 *versus* 9.1 a.f.u. in sample (1); 9.5 *versus* 8.1 a.f.u. in sample (2); 10.3 *versus* 7.8 a.f.u. in sample (3). The discrepancy in sample (3) is too high (*ca* 24%) to be only due to an incorrect assignment of the TG weight loss. There must be a bias in the Rietveld refined occupancy factors of the water molecules probably because of cryptic parameter correlation during the least-square procedures.

The IR patterns are reported in Fig. 3. The characteristic absorption bands of NH_4^+ in the regions labelled *a* and *b* [the

two IR-active triply degenerate vibrations ν_3 and ν_4 (Gadsden, 1975) at 3134 and 1400 cm^{-1}, respectively] clearly increase with the amount of NH_4^+ in the zeolite sample. Table 5 reports the positions of the bands in the IR spectra.

4. Discussion

In a family of phillipsites with different *R*, exchanged with a cation (say K^+, for example), an increase in the population of site I results in a stretch of the corresponding O—*T* distances and consequently a net increase in the size of the tetrahedra (Gualtieri *et al.*, 1999*a*). This behaviour is not observed here because all samples display a full occupancy of site I and very similar average *T*—O distances [1.65 (2)–1.66 (4) Å]. Despite the bland scatter of the average *T*—O distances, the standard uncertainty of the *T*—O distances tends to decrease with *R*: 0.038 Å in sample (1), 0.021 Å in sample (2) and 0.021 Å in sample (3), respectively. This is in accordance with the trend depicted in Fig. 4, showing that tetrahedra become less distorted as the Al content decreases. The contribution of the NH_4^+—O interaction to the distortion appears to be minor, because only NH_4^+ in site II is expected to interact differently with the framework O atoms owing to the variation of the site population. Moreover, in sample (1) with more NH_4^+, the longer *T*—O distances in the tetrahedra involving the O atoms bonded to the N atoms are only *T*2—O6 at 1.733 (6) Å and *T*4—O6 at 1.720 (5) Å, with O6 coordinated to N in site II at 3.07 (2) Å (Table 4). The charge-oversaturated O6 bonded to NH_4^+ moves further away towards (Si,Al), which consequently moves closer to the other coordinated O atoms resulting in a net distortion of the tetrahedron.

The distortions affect some absorption bands in the 690–740 cm^{-1} region of the IR patterns. In zeolites, no vibrations specific to AlO_4 tetrahedra or Al—O bonds are assigned, but rather vibrations of TO_4 groups and *T*—O bonds, where the vibrational frequencies represent the average Si,Al composition (Flanigen *et al.*, 1971). Stretching modes involving motions primarily associated with the *T* atoms (internal tetrahedra) described as *symmetric stretching modes* are assigned in the 650–820 cm^{-1} region. These modes are sensitive to framework Si/Al composition and shift to lower frequencies with increasing Al content. The decrease in frequency is related to variation in bond length and bond order: a longer bond length of Al—O and a decreased electronegativity of Al result in a decrease in the force constant (Stubican & Roy, 1961). The IR patterns clearly show a difference in the shape of the bands at *ca* 700 cm^{-1} assigned to ← OTO → symmetric stretching with *R*: the lower the *R* value, the larger the split of the bands. A linear trend is found between the band shift (see Table 5) and *R* ($[\leftarrow \text{OTO} \rightarrow]_1 = -114R + 811$, with $R^2 = 0.999$, and $[\leftarrow \text{OTO} \rightarrow]_2 = 129R + 607$, with $R^2 = 0.997$), although this is only speculative since it is based on only three data points.

Random substitution of Al for Si in the framework would only induce a shift of the bands at low frequencies. The split is due to some *T*—O distances which become shorter and the corresponding band shift at higher frequency, and other *T*—O distances which become longer and the corresponding band shift at lower frequency. Although it is purely speculative, Fig. 4 may support this explanation. In fact, the spread of the *T*—O distances leads to two possible separated groups of *T*—O distances responsible for the split of the IR absorption bands.

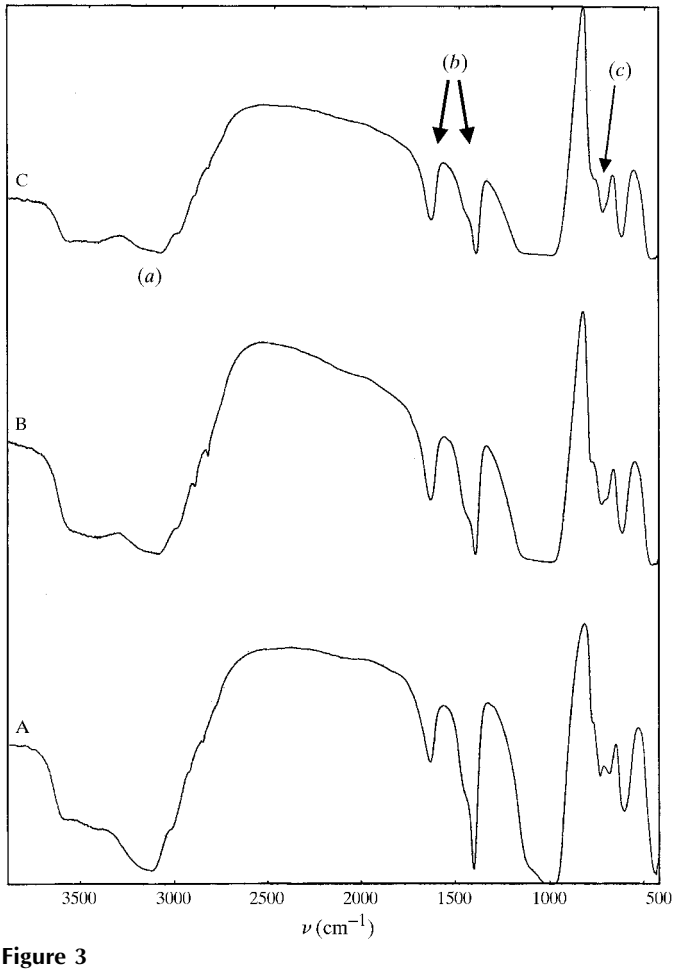

Figure 3
IR patterns of the investigated phillipsite samples. The characteristic absorption bands of NH_4^+, ν_3 and ν_4, are labelled (*a*) and (*b*), respectively. The internal tetrahedra *symmetric stretching* sensitive to framework Si/Al composition is labelled (*c*).

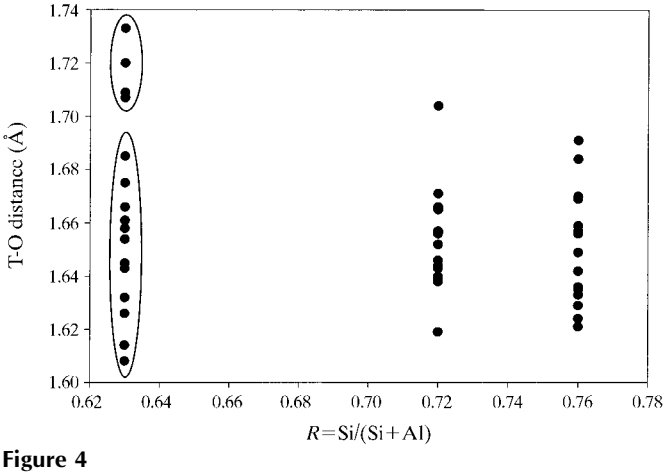

Figure 4
Spread of the *T*—O bond distances in the three phillipsite samples.

Table 4
Significant interatomic distances (Å) involving framework atoms and extra framework cations.

The average is calculated on the basis of the coordinating anions at a bond distance excluding distances which are either too short or > 3.6 Å.

Distance	Sample (1)	Sample (2)	Sample (3)
T1—O2	1.632 (7)	1.656 (6)	1.670 (7)
T1—O3	1.626 (6)	1.638 (7)	1.656 (7)
T1—O5	1.685 (5)	1.666 (6)	1.642 (6)
T1—O7	1.666 (3)	1.639 (3)	1.621 (3)
T2—O2	1.645 (6)	1.640 (5)	1.635 (5)
T2—O3	1.654 (4)	1.643 (4)	1.659 (4)
T2—O6	1.733 (6)	1.704 (4)	1.657 (6)
T2—O8	1.709 (7)	1.671 (7)	1.670 (8)
T3—O1	1.661 (6)	1.652 (7)	1.636 (4)
T3—O4	1.608 (5)	1.619 (8)	1.629 (7)
T3—O5	1.675 (6)	1.665 (6)	1.669 (5)
T3—O7	1.643 (4)	1.619 (3)	1.624 (2)
T4—O1	1.614 (6)	1.646 (7)	1.649 (5)
T4—O4	1.658 (4)	1.644 (4)	1.633 (6)
T4—O6	1.720 (5)	1.657 (7)	1.684 (4)
T4—O9	1.707 (8)	1.671 (4)	1.691 (7)
Average	1.665 (38)	1.652 (21)	1.652 (21)
I—O1 × 2	3.340 (5)	2.906 (6)	3.087 (8)
I—O3 × 2	3.344 (5)	–	3.38 (1)
I—O5 × 2	2.910 (4)	2.994 (5)	3.048 (6)
I—O9	2.927 (5)	3.109 (5)	2.90 (1)
I—O(*W*1)	3.220 (3)	–	–
I—O(*W*2)	–	2.954 (5)	2.74 (1)
I–O(*W*3) × 2	2.609 (11)	2.826 (7)	2.77 (2)
I–O(*W*4)	–	2.855 (5)	2.98 (2)
Average	3.05 (30)	2.93 (9)	3.017 (49)
II–O3	3.32 (3)	3.252 (9)	3.277 (9)
II—O6	3.07 (2)	3.050 (6)	3.007 (6)
II–O7	3.04 (2)	–	–
II—O(*W*1)	–	3.018 (8)	2.96 (1)
II—O(*W*2)	3.49 (2)	3.435 (6)	3.33 (1)
II—O(*W*3)	2.75 (4)	2.969 (7)	3.16 (2)
II—O(*W*3)	3.20 (3)	–	–
II—O(*W*4)	1.52 (2)†	2.233 (6)	2.12 (1)
II—O(*W*5)	2.826 (6)	2.945 (7)	2.946 (9)
Average	3.09 (26)	2.98 (37)	2.97 (40)
HI1···O1 × 2	–	3.37 (2)	3.436 (9)
HI1—O3 × 2	2.92 (2)	3.22 (2)	3.271 (9)
HI1—O5 × 2	2.842 (6)	2.928 (6)	2.992 (6)
HI1—O(*W*1)	3.17 (2)	3.43 (2)	3.144 (8)
HI1—O(*W*2)	2.18 (2)	2.05 (2)†	1.90 (1)†
HI1—O(*W*3) × 2	3.05 (2)	3.437 (8)	3.42 (2)
HI2—O1 × 2	2.80 (5)	2.39 (4)	2.562 (6)
HI2—O5 × 2	3.03 (3)	3.18 (3)	3.245 (7)
HI2—O9	2.42 (7)	2.45 (8)	2.14 (1)
HI2—O(*W*1)	2.48 (3)	2.94 (4)	2.986 (6)
HI2—O(*W*2)	3.04 (6)	3.34 (7)	3.33 (1)
HI2—O(*W*3) × 2	3.31 (4)	3.22 (4)	3.13 (3)
HI2—O(*W*4)	–	3.13 (3)	3.05 (2)
HI3—O1	3.05 (1)	2.64 (1)	2.86 (8)
HI3—O3	2.93 (2)	3.05 (2)	2.76 (8)
HI3—O5	2.41 (2)	2.43 (2)	2.46 (1)
HI3—O8	–	3.40 (1)	3.25 (8)
HI3—O9	2.95 (3)	3.23 (2)	3.12 (8)
HI3—O(*W*2)	–	3.37 (3)	3.05 (4)
HI3—O(*W*3)	2.50 (2)	3.00 (2)	2.95 (2)
HI3—O(*W*3)	1.98 (2)†	2.00 (2)†	1.98 (3)†
HI3—O(*W*4)	–	2.51 (2)	2.72 (3)
HII1—O3	3.32 (2)	2.99 (4)	3.40 (1)
HII1—O3	–	3.42 (3)	3.04 (1)
HII1—O4	3.27 (1)	–	–
HII1—O6	–	3.41 (2)	3.379 (9)
HII1—O7	3.03 (2)	3.44 (2)	3.46 (1)
HII1—O(*W*2)	2.66 (1)	2.54 (2)	2.46 (1)
HII1—O(*W*3)	3.07 (3)	3.29 (4)	–
HII1—O(*W*3)	3.26 (3)	–	–
HII1—O(*W*4)	2.03 (2)†	2.23 (4)	2.15 (2)
HII1—O(*W*5)	–	3.47 (2)	3.50 (1)
HII2—O1	–	3.41 (2)	–
HII2—O3	2.58 (3)	2.75 (2)	2.77 (1)
HII2—O6	2.47 (2)	2.15 (2)	2.101 (9)
HII2—O6	–	3.45 (4)	3.39 (1)
HII2—O7	2.48 (7)	–	–
HII2—O8	–	–	3.44 (1)
HII2—O9	–	3.44 (1)	–
HII2—O(*W*1)	–	3.26 (2)	3.18 (1)
HII2—O(*W*3)	3.43 (4)	–	–
HII2—O(W4)	2.17 (8)	3.13 (2)	3.02 (2)
HII2—O(*W*5)	2.34 (10)	2.70 (4)	2.70 (1)
HII3—O6	2.85 (1)	3.47 (1)	3.24 (1)
HII3—O6	3.23 (2)	3.44 (1)	–
HII3—O(*W*1)	3.27 (2)	2.33 (2)	2.29 (1)
HII3—O(*W*3)	3.08 (2)	3.09 (1)	2.99 (2)
HII3—O(*W*3)	2.91 (2)	3.13 (1)	3.38 (2)
HII3—O(*W*4)	0.77 (2)†	2.14 (1)	2.02 (2)†
HII3—O(*W*5)	–	–	3.17 (1)
HII4—O4	3.24 (2)	–	–
HII4—O6	–	3.488 (8)	3.444 (8)
HII4—O7	3.15 (2)	3.35 (1)	3.30 (1)
HII4—O(*W*1)	–	3.05 (1)	3.06 (1)
HII4—O(*W*3)	1.97 (3)†	2.155 (9)	2.41 (3)
HII4—O(*W*3)	2.77 (2)	–	–
HII4—O(*W*4)	1.73 (2)†	1.99 (1)†	1.89 (2)†
HII4—O(*W*5)	2.55 (1)	2.36 (1)	2.37 (1)
Average H—O	2.47 (6)	2.50 (15)	2.62 (13)
Average H—O(*W*)	2.55 (14)	2.44 (17)	2.58 (30)
Average	2.51 (12)	2.47 (15)	2.55 (16)
II′—O3	2.51 (3)	2.541 (7)	2.53 (36)
II′—O4	3.32 (2)	2.924 (6)	3.13 (2)
II′—O6	3.20 (1)	3.395 (4)	3.26 (2)
II′—O7	2.502 (7)	2.50 (1)	2.49 (3)
II′—O(*W*2)	2.50 (1)	2.461 (8)	2.46 (39)
II′—O(*W*3)	–	3.104 (7)	3.46 (6)
II′—O(*W*4)	2.52 (3)	2.540 (8)	2.53 (42)
II′—O(*W*5)	3.40 (1)	2.872 (9)	2.80 (3)
Average	2.508 (9)	2.60 (21)	2.50 (3)

† Sites too close to be simultaneously occupied.

Other possible explanations, such as the formation of hydrogen bonds to the framework and the distortion of the tetrahedra, have been unsuccessfully explored. A neutron diffraction study should be performed to this aim, since it gives a better picture of the hydrogen-bonding system.

Fig. 5 shows the position and orientation of the NH_4^+ ions in the phillipsite cages. In site I, two protons (HI1 and HI2) and the nitrogen lie on the mirror plane, while HI3 is in a general position. The ion in site II is in a general position. Given the short II—II′ distance, site II′ is occupied by residual sodium only when site II is empty.

In all the samples, nitrogen at site I is within bonding distance of seven framework O atoms and four water molecules at an average distance of 3.1 (3) Å in sample (1), 2.93 (9) Å in sample (2) and 3.02 (5) Å in sample (3), respectively. Nitrogen at site II is within bonding distance of three framework O atoms and three water molecules at an average distance of 3.1 (3) Å in sample (1), 3.0 (4) Å in sample

Table 5
Assignment and position (cm^{-1}) of the absorption bands in the IR spectra of NH_4-exchanged phillipsites.

Assignment	Sample (1) [*A* in Fig. 3]	Sample (2) [*B* in Fig. 3]	Sample (3) [*C* in Fig. 3]	Label in Fig. 3
NH_4-$\upsilon_3(f2)$	3131	3141	3131	(*a*)
NH_4-$\upsilon_2(e)$	1640	1645	1645	(*b*)
NH_4-$\upsilon_4(f2)$	1465	1460	1461	
	1406	1407	1406	
← OTO →	739	729	724	(*c*)
Symmetric stretch	689	700	706	

(2) and 3.0 (4) Å in sample (3), respectively. These coordination data are comparable to those reported by Yang & Armbruster (1998) for heulandite, albeit fairly lower for site II. This may be explained by a much larger number of water molecules in the latter. It is confirmed here that generally the N—O distances are larger than N—W because neutral water molecules have more freedom to approach the ammonium ions and minimize the electrostatic energies of the whole geometrical configuration with respect to the ammonium ions (and extraframework cations) which must be located in the equilibrium centre of the negative charges of the framework, as inferred by Yang & Armbruster (1998). Figs. 6(*a*) and (*b*) show the chemical environment of the N atoms in sites I and II for sample (1).

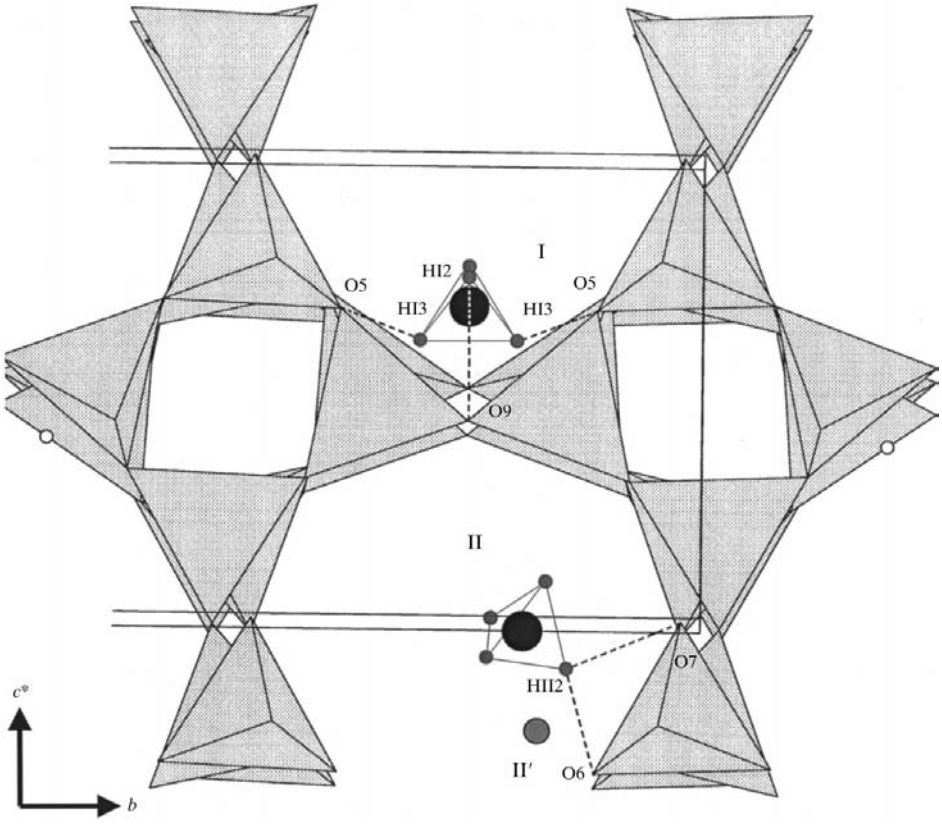

Figure 5
The position of the NH_4^+ tetrahedra in sites I and II. The position of site II′ occupied by sodium is also shown. Dashed lines represent the hydrogen bonds connecting the framework O atoms. Water molecules and relative interactions with H atoms of the NH_4^+ ions are not shown.

An increase in cell volume with NH_4^+ content is observed [from 1008.7 (3) $Å^3$ in sample (3) to 1019.0 (9) $Å^3$ in sample (1)]. The increase is in concert with that observed for NH_4^+-exchanged stilbite and stellerite (Martucci *et al.*, 1999; Alberti *et al.*, 1999*a*,*b*). It is impossible, however, to separate the contribution of NH_4^+ and Al to the increase in cell volume. As the number of NH_4^+ ions decreases, more space is left for water molecules and in fact sample (3) has 2.59 H_2O with respect to sample (1) with 2.32 H_2O. Site O(*W*4) at the centre of the cage of type II is too close to NH_4^+ in site II and the two sites cannot be simultaneously occupied. The same applies to Na^+ in site II′, *i.e.* statistically when site II is empty, O(*W*4) and II′ sites are populated. Although it has no statistical meaning, the average bond lengths involving the H atoms of the NH_4^+ ions reported in Table 4 seem to indicate that hydrogen bonds formed by acceptor water O atoms are stronger than those formed by acceptor framework O atoms, as already postulated in Yang & Armbruster (1998).

The nature of the Brönsted and Lewis acid sites on acid catalysis and the estimate of their concentrations can be performed using a chemi-adsorbed molecular probe, such as NH_3 and NH_4^+ (Yin *et al.*, 1997). Diffraction studies may be a great help to spectroscopy since they clearly elucidate the nature of the geometry of the local siting of the ammonium ion for which mono-, bi-, tridentate or even more complex structures might be formed (Zecchina *et al.*, 1997). Very stable adducts are formed here between NH_4^+ and the Brönsted sites since a progressive decrease of the broad band around 3500 cm^{-1} is observed from sample (1) to sample (3) in Fig. 2, in agreement with the results reported in Geobaldo *et al.* (1995) where an ammonia decrease leads to an erosion of the bands associated with the strong Brönsted acid sites in the region around 3500 cm^{-1}. *Ab initio* calculations for the simulation of IR patterns in the 1300–3700 cm^{-1} region have been performed for the different local symmetries of NH_4^+ in various zeolitic fragments (Zecchina *et al.*, 1997). The absorption bands in the 1400–1700 cm^{-1} region attributed to $\upsilon_4(f2)$ and $\upsilon_2(e)$ vibrations are particularly sensitive to such changes. In that region (labelled *b* in Fig. 3) there are two bands: one at *ca* 1650 cm^{-1} and a split band at *ca* 1380 cm^{-1}. The number and shape of these bands is similar to either simulation (*b*) (monodentate structure) or (*d*) (tridentate structure) reported in Fig. 1 of Zecchina *et al.* (1997). Monodentate structure indicates that one H atom out of four interacts with one framework

oxygen, while tridentate has three out of four H atoms interacting with three different framework O atoms. Although the *ab initio* IR simulations were performed for Si/Al ordered configurations, while phillipsite clearly shows a very low degree of Si/Al ordering, we can make a comparison with our diffraction data (Tables 4 and 6). The relevant geometric data concerning the hydrogen bonding of NH_4^+ are given in Table 6.

Although water H atoms cannot be localized, it is possible to give some indications on their possible orientation and on the environment of the water molecules. Water H atoms of O(*W*1) should be oriented towards O2: O(*W*1)—O2 3.161 (5) Å in sample (1), 3.042 (4) Å in sample (2) and 2.919 (4) Å in sample (3), respectively; alternatively towards O8: O(*W*1)—O8 2.748 (8) Å in sample (1), 2.709 (13) Å in sample (2) and 3.05 (13) Å in sample (3), respectively. Moreover, O(*W*1) shows interactions with other water molecules. Sample (1): O(*W*1)—O(*W*2) 2.882 (4), O(*W*1)—O(*W*3) 3.296 (9) and O(*W*1)—O(*W*4) 2.58 (2) Å; sample (2): O(*W*1)—O(*W*4) 3.375 (7) Å; sample (3): O(*W*1)—O(*W*4) 3.27 (4) Å.

O(*W*2), at the centre of the cage of type I, is loosely bridged to the framework and water H atoms should be oriented towards O4: O(*W*2)—O4 3.245 (3) Å in sample (1) and 3.102 (6) Å in sample (2); or towards O3 in sample (3): O(*W*2)—O3 3.248 (4) Å. Water H atoms of O(*W*3) are probably disordered over many positions since a number of connections with the framework are possible: O(*W*3)—O2 3.15 (1) Å in sample (1), 3.192 (5) Å in sample (2) and 2.80 (6) Å in sample (3), respectively; O(*W*3)—O3 3.16 (2) Å in sample (1), 3.461 (6) Å in sample (2) and 2.97 (4) Å in sample (3), respectively; O(*W*3)—O5 3.070 (6) Å in sample

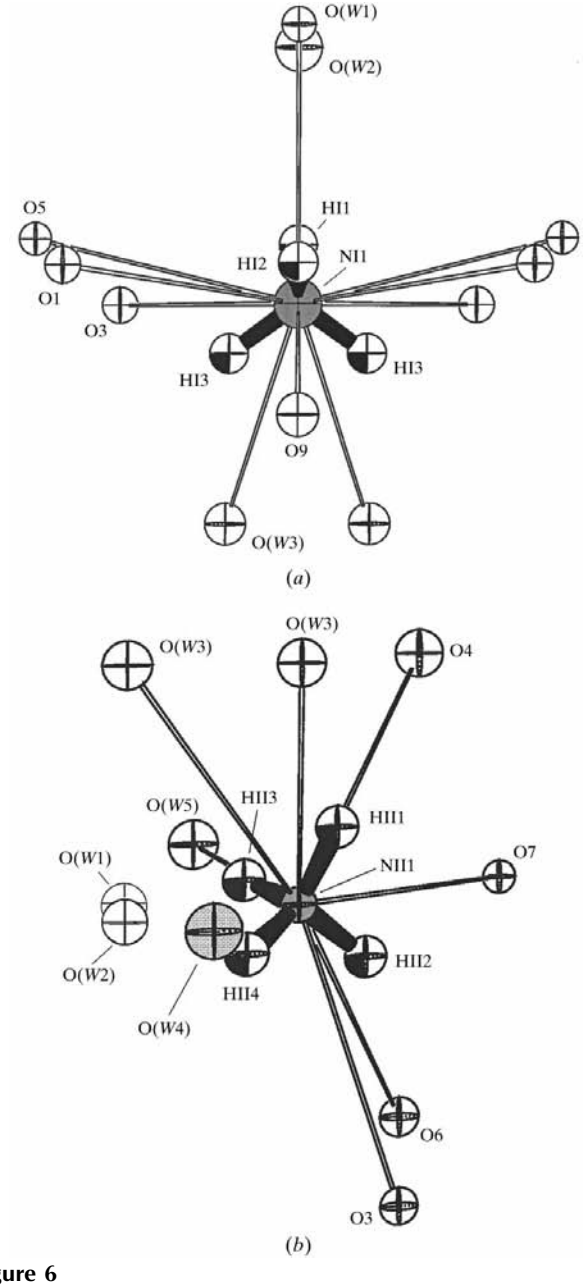

Figure 6
Example of the local symmetry of NH_4^+ in (*a*) site I and (*b*) site II in sample (1). H atoms are represented as balls with one black quadrant. Site O(*W*4) (grey) is too close to nitrogen and is empty when site II is populated.

Table 6
Geometry of the hydrogen bonds formed by the NH_4^+ ion in sites I and II.

First row: sample (1); second row: sample (2); third row: sample (3).

	H···*A* (Å)	*D*···*A* (Å)	*D*—H···*A* (°)
NI2—HI1···O(*W*2)	2.18	2.975 (4)	147
	2.05	2.954 (5)	177
	1.90	2.74 (1)	157
NI2—HI2···O1	–	–	–
	2.39	2.906 (6)	116
	2.56	3.087 (8)	118
NI2—HI2···O9	2.42	2.927 (5)	116
	2.45	3.109 (5)	131
	2.14	2.90 (1)	142
NI2—HI2···O(*W*1)	2.48	3.220 (3)	139
	–	–	–
	–	–	–
NI2—HI3···O(*W*3)	1.98	2.609 (11)	125
	2.00	2.826 (7)	151
	1.98	2.78 (2)	147
NI2—HI3···O5	2.41	2.910 (4)	115
	2.43	2.994 (6)	121
	2.46	3.048 (6)	124
NII4—HII1···O(*W*2)	2.66	3.49 (2)	154
	2.54	3.435 (7)	167
	2.46	3.327 (11)	163
NII4—HII2···O(*W*5)	2.34	2.826 (6)	114
	–	–	–
	–	–	–
NII4—HII2···O3	2.58	3.32 (3)	139
	–	–	–
	–	–	–
NII4—HII2···O6	2.47	3.07 (2)	124
	2.15	3.049 (6)	175
	2.10	3.007 (06)	175
NII4—HII2···O7	2.48	3.04(2)	121
	–	–	–
	–	–	–
NII4—HII3···O(*W*1)	–	–	–
	2.33	3.018 (8)	132
	2.29	2.961 (11)	167
NII4—HII4···O(*W*5)	–	–	–
	2.36	2.945 (7)	121
	2.37	2.946 (09)	121
NII4—HII4···O(*W*3)	1.97	2.75 (4)	144
	2.16	2.969 (7)	146
	2.40	3.16 (2)	141

(2) and 3.09 (2) Å in sample (3), respectively; O(*W*3)—O8 2.63 (2) Å in sample (1), 3.452 (6) Å in sample (2) and 3.07 (5) Å in sample (3), respectively. O(*W*3) also displays a number of interactions with other water molecules. In sample (1), O(*W*3)—O(*W*4) 2.59 (2) Å with the short contact O(*W*3)—O(*W*3) 1.56 (2) Å, which excludes a simultaneous occupation. In sample (2), O(*W*3)—O(*W*3) 3.38 (3) and O(*W*3)—O(*W*5) 3.271 (9) Å with the short contact O(*W*4) 1.894 (10) Å. In sample (3) there are interactions from O(*W*3) to O(*W*1) at 3.45 (3), O(*W*3) at 3.227 (2), O(*W*4) at 2.06 (4) and O(*W*5) at 3.45 (2) Å.

O(*W*4), at the centre of the cage of type II, is connected to cations in sites I and II, and loosely connected to the framework O atoms. In fact, the only possible connection of the water H atoms with the framework is with O9 at 3.099 (6) Å in sample (2) and 2.88 (9) Å in sample (3).

O(*W*5), on a symmetry centre, is bridged to O7 [at 2.968 (3) Å in sample (1), 2.923(3) Å in sample (2) and 2.860 (3) Å in sample (3), respectively] *via* disordered H atoms.

By the nature (ionic radius and charge) and coordination number of the cation in site II, it is possible to predict whether or not site II′ is populated. When the *atomic sterical occupancy* coefficient *C* (defined in Gualtieri *et al.*, 1999, as the product of the atomic charge *c*, its ionic radius *r* and the average cation–anion distance *d*) is larger than 5.73 (as in the case of Sr^{2+} and Ba^{2+}) site II′ is not populated since the negative charge density at the bottom of the cage is already balanced by such large doubly charged cations. When *C* is lower than 5.73 (as in the case of Ca^{2+} and Na^{+}), Na^{+} in site II′ is needed to achieve a balance of positive charge in the cage. In NH_4^{+}-exchanged phillipsites *C* is 4.54 (assuming an ideal ionic radius of 1.46 for nitrogen), indicating that Na^{+} should be found in site II′. The refinements actually show electron density at site II′ in all the samples, in agreement with the microprobe analysis indicating that some sodium is retained in the structure after the $NH_4^{+} \rightarrow Na^{+}$ exchange. Surprisingly, analytical sodium in sample (2) seems to be underestimated. This may be due to an effect of cation migration taking place under the electron beam.

5. Conclusions

Cation exchange by NH_4^{+} can be considered complete in phillipsite. NH_4^{+} is refined in sites I and II and some residual sodium is refined in site II′. NH_4^{+} in site I shows three H atoms interacting with O atoms of the framework and a number of interactions with water O atoms. In all three samples, monocentric and dicentric connections are formed. NH_4^{+} in site II shows a structure with one H atom interacting with O atoms of the framework and a number of interactions with water O atoms. In sample (1) two monocentric connections and a quadricentric one were found, in sample (2) three dicentric connections and a monocentric one were found, and in sample (3), three monocentric connections and a dicentric one were formed.

This work is part of a research project involving E. Passaglia and E. Galli, whose help in sample selection and preparation is greatly acknowledged. J. C. Hanson helped during data collection at X7B (NSLS, BNL) under contract DE-AC02-76CH00016 with the US Department of Energy by its Division of Chemical Science, Office of Basic and Energy Sciences. Financial support is acknowledged from the Italian MURST. A. Alberti is greatly acknowledged for critical reading of the manuscript, and M. Panzalorto and P. L. Fabbri for collection of the IR spectra. G. Vezzalini and T. Giliberti performed the chemical analyses.

References

Alberti, A., Martucci, A., Sacerdoti, M., Quartieri, S., Vezzalini, G., Ciambelli, P. & Rapacciuolo, M. (1999*a*). *Proc. XII IZA Conf.*, 5–10 July 1998. Baltimore, MA, USA.

Alberti, A., Martucci, A., Sacerdoti, M., Quartieri, S., Vezzalini, G., Ciambelli, P. & Rapacciuolo, M. (1999*b*). *Mater. Res. Soc.* pp. 2345–2354.

Amemija, Y. (1990). *Synchrotron Rad. News*, **3**, 21–26.

Dinnebier, R. E. (1999). *Powder Diff.* **14**, 84–92.

Donovan, J. J. (1995). *Advanced Microbeam.* 4217C Kings Graves Road, Vienna, OH 44473, USA.

Flanigen, E. M., Khatami, H. & Szymansky, H. A. (1971). *Adv. Inorg. Chem. Ser.* **101**, 201–229.

Gadsden, J. A. (1975). *Infrared Spectra of Minerals and Related Inorganic Compounds*, p. 277. London: Butterworths.

Geobaldo, F., Lamberti, C., Ricchiardi, G., Bordiga, S., Zecchina, A., Turnes Palomino, G. & Otero Areán, C. (1995). *J. Phys. Chem.* **99**, 11167–11173.

Gottardi, G. & Galli, E. (1985). *Natural Zeolites*, p. 409. Berlin: Springer Verlag.

Gualtieri, A. F., Caputo, D. & Colella, C. (1999). *Microporous Mesoporous Mater.* **32**, 319–329.

Gualtieri, A. F., Norby, P., Hanson, J. C. & Hriljac, J. (1996). *J. Appl. Cryst.* **29**, 707–713.

Gualtieri, A. F., Passaglia, E. & Galli, E. (1999*a*). *Proc. of Zeolite 97 Intl Conf.* In the press.

Gualtieri, A. F., Passaglia, E. & Galli, E. (1999*b*). *Microporous Mesoporous Mater.* **31**, 33–43.

Hastings, J. B., Suortii, P., Thomlinson, W., Kvick, Å. & Koetzle, T. F. (1983). *Nucl. Instrum. Methods*, **208**, 55–58.

Larson, A. C. & Von Dreele, R. B. (1999). *LAUR. Generalized Structure Analysis System*, p. 179. Los Alamos, New Mexico.

Lightfoot, P., Metha, M. A. & Bruce, P. G. (1993). *Science*, **262**, 883–885.

Martucci, A., Alberti, A., Sacerdoti, M., Vezzalini, G., Ciambelli, P. & Rapacciuolo, M. (1999). *Proc. of Zeolite 97 Intl Conf.* In the press.

Norby, P. (1997). *J. Appl. Cryst.* **30**, 21–30.

Passaglia, E., Gualtieri, A. F. & Galli, E. (1999). *Proc. of Zeolite 97 Intl Conf.* In the press.

Rinaldi, R., Pluth, J. J. & Smith, J. V. (1974). *Acta Cryst.* B**30**, 2426–2433.

Sadanaga, R., Marumo, F. & Takéuchi, Y. (1961). *Acta Cryst.* **14**, 1153–1163.

Schreinger, A. (1963). *Acta Cryst.* **16**, 546–550.

Steinfink, H. (1962). *Acta Cryst.* **15**, 644–651.

Stubican, V. & Roy, R. (1961). *Am. Mineral.* **46**, 32–51.

Yang, P. & Armbruster, T. (1998). *Eur. J. Mineral.* **10**, 461–471.

Yin, F., Blumenfeld, A. L., Gruver, V. & Fripiat, J. J. (1997). *J. Phys. Chem.* **101**, 1824–1830.

Zecchina, A., Marchese, L., Bordiga, S., Pazè, C. & Giannotti, E. (1997). *J. Phys. Chem.* **101**, 10128–10135.